International Journal for Parasitology: Drugs and Drug Resistance xxx (xxxx) 100634

Contents lists available at ScienceDirect

International Journal for Parasitology: Drugs and Drug Resistance

journal homepage: www.elsevier.com/locate/ijpddr

Meclonazepam sensitivity of parasitic flatworms correlates with $TRPM_{MCLZ}$ sensitivity to meclonazepam

Claudia M. Rohr [a], Paul McCusker [b], Marc Kaethner [c, d], Rebecca Armstrong [b], Emily Robb [b], Sang-Kyu Park [a], Daniel J. Sprague [a, 1], Aaron G. Maule [b], Mostafa Zamanian [f], Britta Lundström-Stadelmann [c, e], John D. Chan [f, g, *], Jonathan S. Marchant [a, **]

[a] Department of Cell Biology, Neurobiology, and Anatomy, Medical College of Wisconsin, Milwaukee, WI, 53226, USA
[b] Understanding Health & Disease, School of Biological Sciences, Queen's University Belfast, Belfast, BT9 5DL, UK
[c] Institute of Parasitology, Department of Infectious Diseases and Pathobiology, Vetsuisse Faculty, University of Bern, 3012, Berne, Switzerland
[d] Graduate School for Cellular and Biomedical Sciences, University of Bern, 3012, Berne, Switzerland
[e] Multidisciplinary Center for Infectious Diseases, University of Bern, 3012, Berne, Switzerland
[f] Department of Pathobiological Sciences, University of Wisconsin - Madison, Madison, WI, USA
[g] Global Health Institute, University of Wisconsin - Madison, Madison, WI, USA

ARTICLE INFO

Keywords:
Transient receptor potential channel
Benzodiazepine
Trematode
Tapeworm

ABSTRACT

The ionotropic portfolio of parasitic flatworms affords considerable opportunity for development of new anthelmintics. In this regard, transient receptor potential ion channels (TRP channels), cation channels responsive to various physiochemical cues, have emerged as promising druggable targets. This is based on the recent discovery that two members of a TRP channel subfamily (TRP melastatin or TRPM channels) are selectively activated by the clinical drug praziquantel ($TRPM_{PZQ}$), or the anthelmintic benzodiazepine meclonazepam ($TRPM_{MCLZ}$). Here, the efficacy of meclonazepam was investigated in a trematode (the liver fluke, *Fasciola hepatica*) and a cestode (*Echinococcus multilocularis*) model, in which an observed lack of meclonazepam sensitivity correlated with the lack of efficacy of meclonazepam on $TRPM_{MCLZ}$ in these different parasites. Such correlations support assignment of $TRPM_{MCLZ}$ as the meclonazepam target. Bioinformatic analysis of all available parasitic flatworm genomes allowed prediction of the meclonazepam binding pocket in over sixty different $TRPM_{MCLZ}$ orthologs. Mutagenesis and functional profiling analyses highlighted the importance of a key residue in the S4 transmembrane helix of $TRPM_{MCLZ}$ that impacts meclonazepam potency and efficacy. Variation of this residue and overall binding pocket architecture between different parasitic flatworm $TRPM_{MCLZ}$ orthologs restricts meclonazepam action to a subset of schistosome species.

1. Introduction

Transient receptor potential ion channels of the melastatin subfamily (TRPM) have emerged as promising targets for anthelmintics (Sprague et al., 2024). This interest is based upon the discovery of two different flatworm TRPM channels that are activated by the antiparasitic drug praziquantel (PZQ, with the target named $TRPM_{PZQ}$ (Andrews et al., 1983; Park et al., 2019),), or the anthelmintic benzodiazepine meclonazepam (MCLZ, with the target named $TRPM_{MCLZ}$ (Stohler, 1979; Park et al., 2024),). Both these ligands have long recognized anthelmintic activity, with PZQ being deployed for decades as the treatment for schistosomiasis as well other clinical and veterinary diseases caused by parasitic flatworms (Andrews et al., 1983). The targets of PZQ and MCLZ that underpin their antiparasitic action had remained a mystery until the recent identification of $TRPM_{PZQ}$ and $TRPM_{MCLZ}$ (Sprague et al., 2024).

For $TRPM_{PZQ}$, unmasked as a PZQ target in 2019 (Park et al., 2019), evidence supporting correct target validation has accumulated through efforts to define the basic properties of the channel *in vitro*, the phenotypic effects of other $TRPM_{PZQ}$ modulators, and genetic studies that demonstrated an association with lower parasite sensitivity to PZQ (reviewed by (Marchant, 2024)). Target validation has also been sup-

* Corresponding author. Department of Pathobiological Sciences, University of Wisconsin - Madison, Madison, WI, USA.
** Corresponding author.
E-mail addresses: jchan32@wisc.edu (J.D. Chan), jmarchant@mcw.edu (J.S. Marchant).
[1] Current address: Department of Biochemistry and Molecular Biology, Medical University of South Carolina, Charleston, SC, 29425, USA.

https://doi.org/10.1016/j.ijpddr.2026.100634
Received 10 September 2025; Received in revised form 15 January 2026; Accepted 16 January 2026
2211-3207/

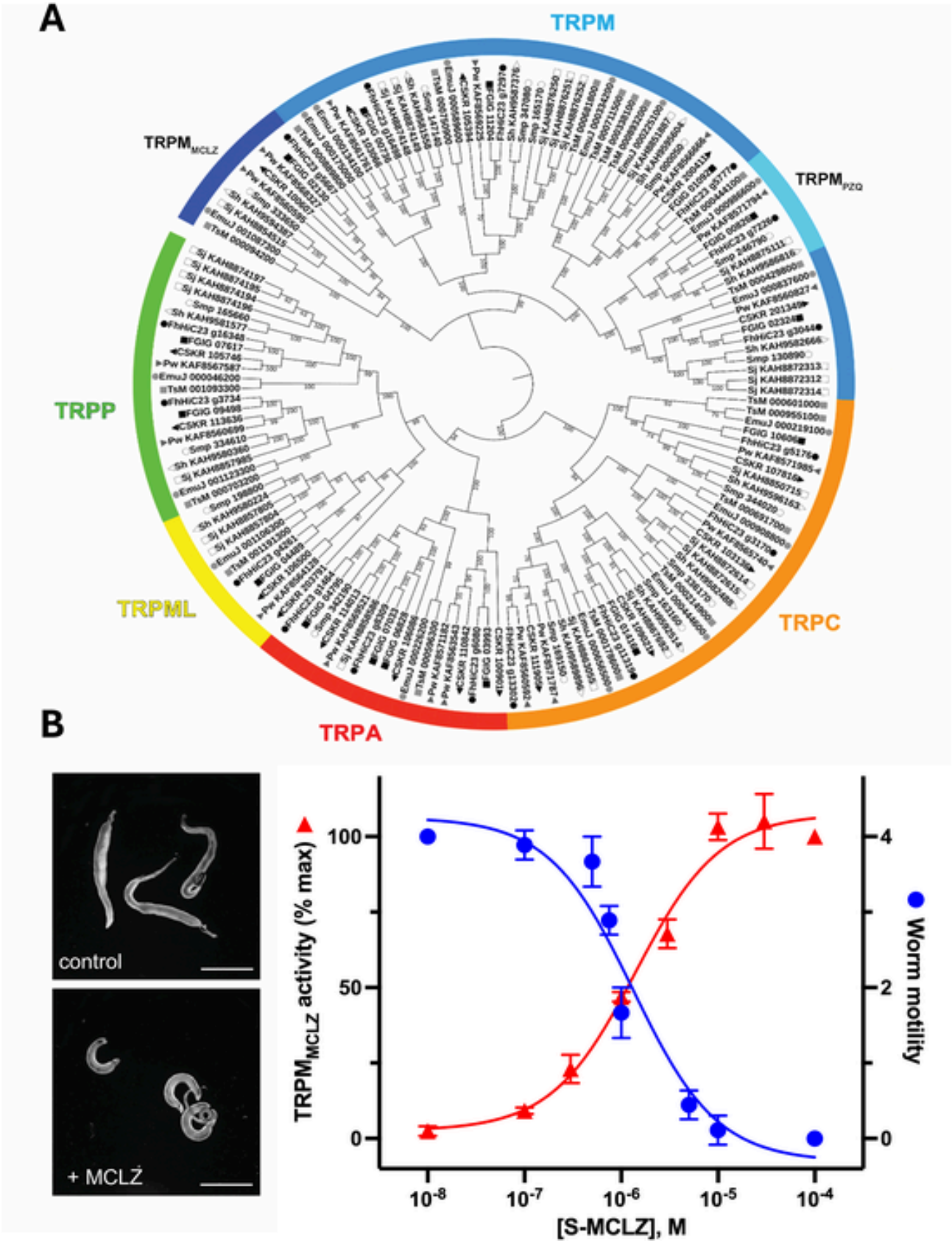
A
TRPM
TRPM$_{MCLZ}$
TRPM$_{PZQ}$
TRPP
TRPML
TRPC
TRPA
B
control
+ MCLZ
TRPM$_{MCLZ}$ activity (% max)
Worm motility
100
50
0
4
2
0
10^{-8}
10^{-7}
10^{-6}
10^{-5}
10^{-4}
[S-MCLZ], M

Fig. 1. Phylogeny of flatworm TRP channels and activity of (*S*)-MCLZ versus *S. mansoni* worms and the target ion channel, $TRPM_{MCLZ}$. (**A**) Phylogenetic analysis of predicted TRP channels from flatworm species across different classes of parasites. Flatworm sequences used in this tree are provided in Supplemental Dataset 1. Shapes represent different parasite species: *Schistosoma mansoni* (open circle), *Schistosoma haematobium* (open square), *Schistosoma japonicum* (open triangle), *Fasciola hepatica* (solid circle), *Fasciola gigantica* (solid square), *Clonorchis sinensis* (left, solid triangle), *Paragonimus westermani* (right, grey triangle), *Echinococcus multilocularis* (grey square), *Taenia solium* (grey circle). Colors represent different TRP subfamilies, with the TRP channels, $TRPM_{MCLZ}$ (*Smp_333650*) and $TRPM_{PZQ}$ (*Smp_246790*) highlighted. $TRPM_{MCLZ}$ clusters within a clade next to the other TRPM orthologs. Several aspects of the full length $TRPM_{MCLZ}$ sequence diverge from conventional TRPM architecture (Sprague et al., 2024), notably the presence of N-terminal ankyrin repeat domains, so this group could be referred to as 'TRPM-like' given clustering proximal to the other TRPM sequences. (**B**) *Left*, representative image stills showing adult *S. mansoni* worms before (top) and after (bottom) treatment with (*S*)-MCLZ (1 μM, 20 min post treatment). Scale bar represents 2 mm. *Right*, concentration response curves comparing the inhibition of (*S*)-MCLZ on worm motility (blue) with (*S*)-MCLZ activation of *Sm*. $TRPM_{MCLZ}$ (red).

ported from studies of $TRPM_{PZQ}$ orthologs in different parasitic flatworms. $TRPM_{PZQ}$ must be present in parasitic flatworms that respond to PZQ, and there should likely be a correlation between the PZQ sensitivity of a parasite and the PZQ sensitivity of the $TRPM_{PZQ}$ ortholog within that species (Rohr et al., 2023). Indeed, it has been shown that in infections that are clinically resolved by PZQ, the $TRPM_{PZQ}$ orthologs of these parasitic flatworms display high sensitivity to PZQ (Rohr et al., 2023; Sprague et al., 2023a). However, in infections that require higher doses of PZQ, these parasites harbor $TRPM_{PZQ}$ orthologs with lower PZQ sensitivity (Rohr et al., 2023). The starkest correlation derived from studies of *Fasciola* spp. liver fluke, which are insensitive to PZQ. *Fasciola* spp. $TRPM_{PZQ}$ is insensitive to PZQ on account of a specific amino acid within the binding pocket of *Fasciola* spp. $TRPM_{PZQ}$ (Park et al., 2021). A new chemotype that is indifferent to this natural binding pocket variation activates *Fasciola* spp. $TRPM_{PZQ}$ and phenocopies PZQ action (Sprague et al., 2023b). Thus, the sensitivity of $TRPM_{PZQ}$ orthologs in different species closely tracks with established parasite sensitivities to PZQ (Marchant, 2024).

For $TRPM_{MCLZ}$, more recently identified as a MCLZ target (Park et al., 2024), target validation is at an earlier stage. MCLZ activates $TRPM_{MCLZ}$ over a similar concentration range to the action of MCLZ on schistosome worms *in vitro* (Park et al., 2024). These concentrations are lower for those species of schistosomes known to be sensitive to MCLZ (*S. mansoni*, *S. haematobium* (Baard et al., 1979)), but higher in species known to be less sensitive to MCLZ (*S. japonicum* (Stohler, 1979; Pica-Mattoccia et al., 2008),). This differential sensitivity was attributed to amino acid variation within the ligand binding pocket of schistosome $TRPM_{MCLZ}$, where a specific residue (a histidine in the 'high sensitivity' African schistosome clade, but a tyrosine in the 'low sensitivity' Asian schistosome clade) defined $TRPM_{MCLZ}$ sensitivity to MCLZ (Park et al., 2024). Reciprocal mutations at this residue within the different $TRPM_{MCLZ}$ backbones (H946Y in *S. mansoni* $TRPM_{MCLZ}$ versus Y944H in *S. japonicum* $TRPM_{MCLZ}$) interchanged the sensitivity of $TRPM_{MCLZ}$ to MCLZ (Park et al., 2024).

This correlation between the functional properties of different *Schistosoma sp*. $TRPM_{MCLZ}$ orthologs with the sensitivity of different schistosome species to MCLZ is supportive of correct target assignment (Park et al., 2024). However, there is further opportunity to assess whether the 'target' versus 'parasite' correlation of MCLZ sensitivity holds for different parasitic flatworms. *$TRPM_{MCLZ}$* is present in all parasitic flatworms (Park et al., 2024), prompting effort to examine the properties of $TRPM_{MCLZ}$ in other parasites relative to the observed sensitivity of these parasites to MCLZ. Currently there is a paucity of publications addressing MCLZ activity against parasitic flatworms other than schistosomes. Therefore, we examined MCLZ action in two different parasitic flatworms in parallel with an assessment of MCLZ sensitivity of the $TRPM_{MCLZ}$ orthologs in these same models.

2. Materials & methods

Reagents. Chemical reagents were from Sigma, with the exception of (*S*)-MCLZ (Cayman Chemical). Cell culture reagents and Lipofectamine 2000 were from Invitrogen.

Cell Culture and transfection. HEK293 cells (ATCC CRL-1573.3) were authenticated by STR profiling (ATCC) and evaluated for mycoplasma contamination through monthly testing (LookOut® Mycoplasma PCR Detection Kit, Sigma). Cells were cultured in DMEM supplemented with 10 % fetal bovine serum (FBS), penicillin (100 units/ml), streptomycin (100 μg/ml), and L-glutamine (290 μg/ml). Individual TRPM constructs were synthesized by Genscript based on genomic and transcriptomic annotations. For functional profiling of $TRPM_{MCLZ}$ orthologs and schistosome TRPM paralogs, cDNAs encoding each construct (Supplementary Dataset 2) were transiently transfected into cultured cells (3×10^6 cells per 100 mm Petri dish) using Lipofectamine 2000.

Ca^{2+} reporter assays. Ca^{2+} reporter assays were performed using a Fluorescence Imaging Plate Reader ($FLIPR^{TETRA}$, Molecular Devices) as detailed previously (Park et al., 2019, 2024). In brief, HEK293 cells were seeded (20,000 cells/well) in a black-walled clear-bottomed poly-d-lysine coated 384-well plate (Greiner Bio-One, Germany) in DMEM growth media (supplemented with 10 % dialyzed FBS). After 24hrs, the growth medium was exchanged and cells loaded with Ca^{2+} indicator by incubation with Fluo-4 NW (Invitrogen). Plates were then incubated (20 μl per well, 50 min at 37 °C, 10 min at room temperature) in Hank's Balanced Salt Solution (HBSS, 1.26 mM $CaCl_2$, 0.49 mM $MgCl_2$, 0.41 mM $MgSO_4$, 5.33 mM KCl, 0.44 mM KH_2PO_4, 4.17 mM $NaHCO_3$, 137.9 mM NaCl, 0.34 mM Na_2HPO_4, 5.55 mM D-glucose, pH7.4) supplemented with probenecid (2.5 mM) and HEPES (20 mM). Drug dilutions (5x concentration) were prepared in assay buffer, without probenecid and dye, in F-form 384-well plates (Greiner Bio-one, Germany). After loading, the Ca^{2+} assay was performed. Basal fluorescence was monitored for 20s at room temperature, then 5 μl of compound was added, and the signal (raw fluorescence units) monitored for a further 250s. Peak fluorescence increases for each well were normalized to maximum-fold increase over baseline. Except where indicated, all data are presented as mean ± SEM.

***Schistosoma mansoni* motility assays.** Adult schistosomes were isolated from the mesenteric vasculature of female Swiss Webster mice previously infected by the Schistosomiasis Resource Center at the Biomedical Research Institute with *S. mansoni* cercariae (NMRI strain). Animal experiments followed ethical regulations approved by the Medical College of Wisconsin Institutional Animal Care and Use Committee. Harvested schistosomes were washed in ABC169 (Wang et al., 2019) and incubated overnight (37 °C, 5 % CO_2) in vented petri dishes (100 × 25 mm). For concentration response analyses, assays were performed using three adult male worms per well in a twenty-four well dish. Motility was scored for each individual worm on a 0–4 scale, following the WHO-TDR scoring matrix guidelines (Ramirez et al., 2007). Scoring was based on motility resolved 20 min after (*S*)-MCLZ application, with images obtained both prior to and after drug treatment. Images were captured using a Zeiss Discovery v20 stereomicroscope with a QiCAM 12-bit cooled color CCD camera controlled by Image-Pro imaging software (v.11.0.4).

***Fasciola hepatica* motility assays**. Metacercariae of the Kilmarnock (triclabendazole-resistant; used in NEJ trial) or Italian (triclabendazole-susceptible; used in 3-week juvenile trial) strains were

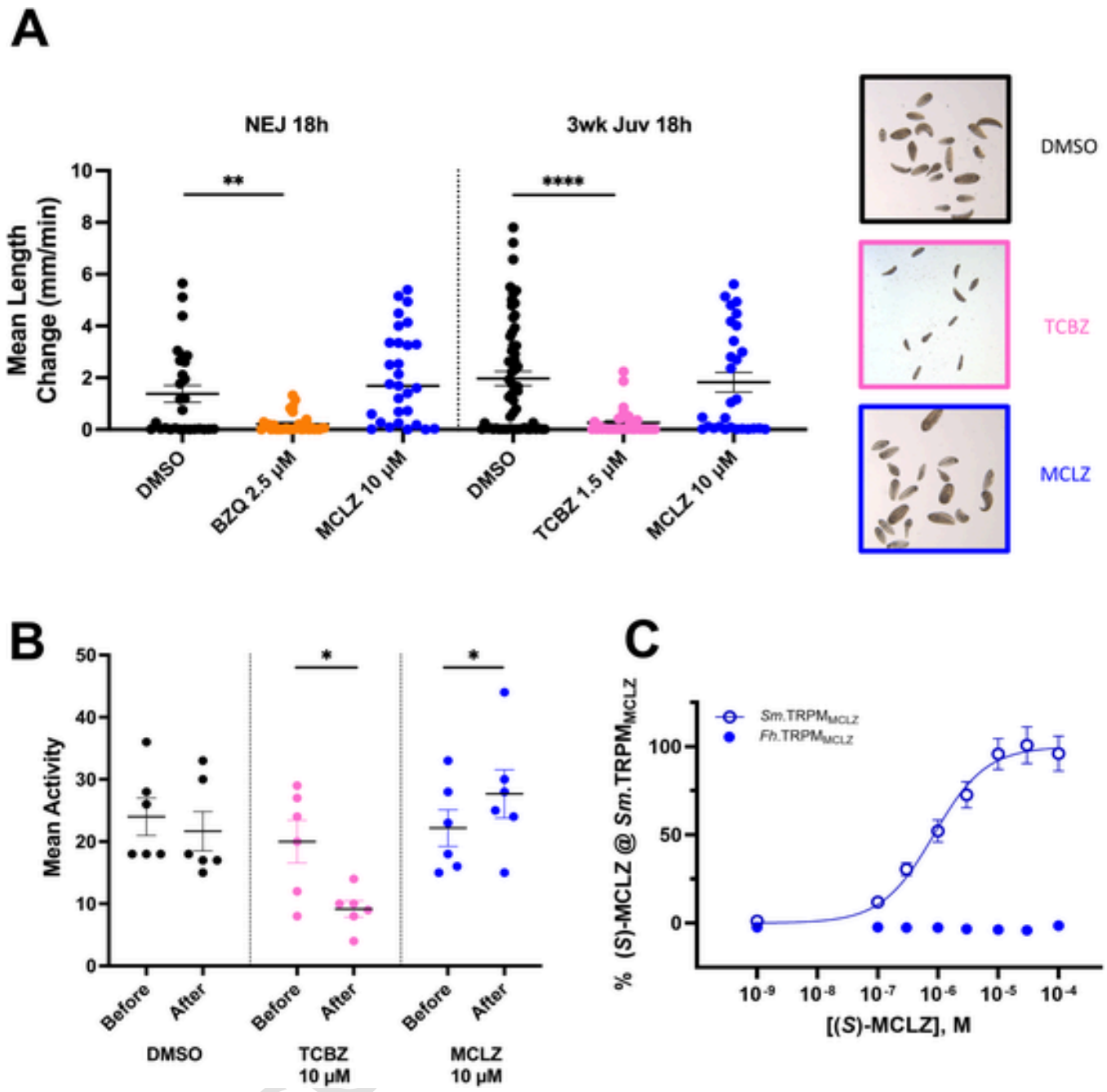

Fig. 2. Activity of (*S*)-MCLZ versus *Fasciola hepatica*. (**A**) *Left*, Length change (mean ± SEM) of *F. hepatica* NEJs 18 h after treatment with BZQ (2.5 µM) or (*S*)-MCLZ (10 µM), **p < 0.01 in a TCBZ-resistant strain. *Middle*, Effects on three-week-old juvenile *F. hepatica* treated with TCBZ (1.5 µM) or MCLZ (10 µM) using a TCBZ-sensitive strain, ****p < 0.0001. *Right*, representative image stills extracted from video recordings of three-week-old juvenile assays. (**B**) *F. hepatica* miracidia activity (mean ± SEM) 15 min prior and 15 min post treatment with TCBZ or (*S*)-MCLZ (both at 10 µM). (**C**) *In vitro* Ca^{2+} reporter assay for *Fasciola hepatica* $TRPM_{MCLZ}$ (*Fh*.$TRPM_{MCLZ}$) compared with *Sm*. $TRPM_{MCLZ}$. Measurements represent peak signal amplitude relative to maximal response of (S)-MCLZ at *Sm*. $TRPM_{MCLZ}$ (mean ± SEM).

purchased from Ridgeway Research (Gloucestershire, UK). These were excysted as described previously (McVeigh et al., 2014; McCusker et al., 2020) with a full protocol available in (McCusker et al., 2023). Compounds for testing were prepared by making 10 mM stocks in DMSO prior to serial dilutions in DMSO. NEJs or three-week-old juveniles cultured in 50 % Chicken serum (McCusker et al., 2016) were moved to 35 mm Petri dishes (82.1135.500, Sarstedt) with 3 ml of RPMI (#11835105, Thermo Fisher Scientific with antibiotic/antimycotic (#A5955, Sigma Aldrich)). Compounds were added such that DMSO was at a final dilution of 1:1000 in all treatments. Benzamidoquinazolinone (BZQ (Sprague et al., 2023b),) or the frontline flukicide triclabendazole (TCBZ) were compared with (*S*)-MCLZ (10 µM). After 18 h the NEJs/three-week-old juveniles were videoed for 1 min under darkfield lighting on an Olympus SC50 camera attached to an Olympus SZX10 microscope. Each drug treatment was carried out in triplicate with replicates carried out on different days. Video analyses were carried out via the wrMTrck plugin (Schneider et al., 2012). Briefly, images were calibrated using a 1 mm scale and the wrMTrck plugin was

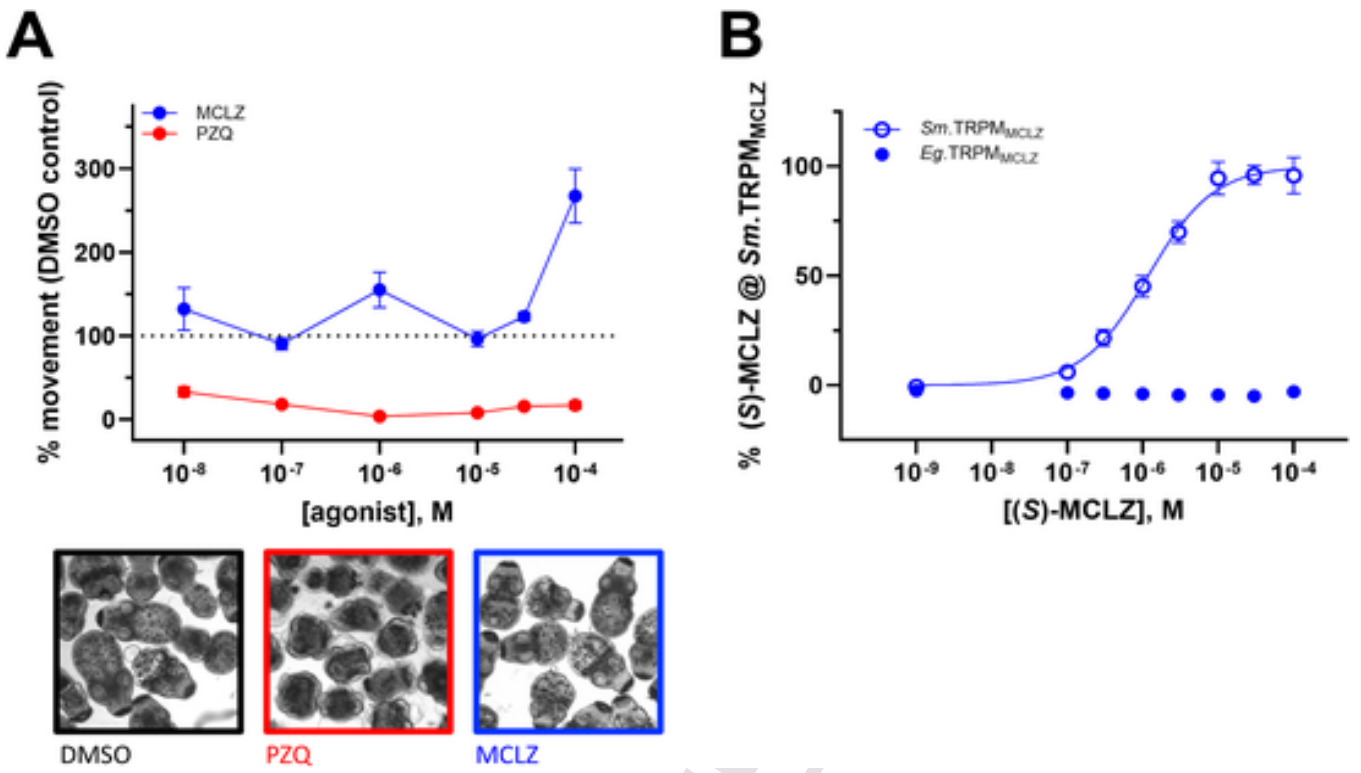

Fig. 3. Activity of (*S*)-MCLZ versus *E. multilocularis* protoscoleces. (**A**) *Top*, Summary of drug assays using *E. multilocularis* protoscoleces. Drug treatments were: (±)-PZQ and (*S*)-MCLZ (both ≤100 μM) for 24hrs. Data are plotted as % motility versus vehicle (DMSO, 0.1 %) control (mean ± SEM). *Bottom*, images of protoscoleces after 24hrs of drug treatment. Contraction and damage was evident in the cohort treated with (±)-PZQ. (**B**) *In vitro* Ca^{2+} reporter assay for *Echinococcus granulosus* $TRPM_{MCLZ}$ (*Eg*.$TRPM_{MCLZ}$) compared with *Sm*. $TRPM_{MCLZ}$. Measurements represent peak signal amplitude relative to maximal response of (S)-MCLZ at *Sm*. $TRPM_{MCLZ}$ (mean ± SEM).

used as default, except for modifications to minSize (10 pixels), maxSize (1000 pixels), maxVelocity (1000 pixels/frame), AreaChange (200 % change in area between frames), Rawdata (2) and benddetect (0). The change in juvenile length between frames was recorded and used to calculate the mean length change of worm/minute from the entire recording. For statistical analyses on the juvenile dataset, a Shapiro-Wilk test was performed for normality, followed by a Kruskal-Wallis test for significance.

To examine miracidia, eggs were collected from infected sheep at a local abattoir (Linden ABP Foods Dungannon, UK). Eggs were washed several times in spring water before being left in Petri dishes in the dark for 2 weeks at 21 ˚C to embryonate. Once embryonated miracidia were exposed to light to trigger hatching. Groups of 10 miracidia were collected in 50 μl water and placed in a 96-well plate. Miracidial movement was recorded for 15 min using the wMicroTracker (InVivo Biosystems, USA) to ascertain baseline movement prior to the addition of compounds. (*S*)-MCLZ and TCBZ were used at final concentration of 10 μM. Six replicates were used for each treatment and the final concentration of DMSO was 1:1000 following serial dilutions in DMSO prior to dilutions in spring water. Activity in each well was recorded as the number of times the laser beam was broken across 5 min. For statistical analyses, a Shapiro-Wilk test was performed for normality, followed by paired t-tests for significance.

Cestode motility assays. Protoscoleces of *E. multilocularis* strain MB17 were isolated from metacestode material grown in experimentally infected gerbils (kindly provided by Prof. Dr. K. Brehm, University of Würzburg). Extraction, activation of protoscoleces, as well as motility assays were performed as outlined previously (Kaethner et al., 2023). Briefly, protoscoleces were activated by 10 % DMSO (3 h at 37 ˚C in a humid atmosphere with 5 % CO_2) and left to recover at 37 ˚C overnight in DMEM with 10 % FBS (Biochrom, Berlin, Germany). The following day, 25 protoscoleces were distributed into individual wells of a white, flat-bottom 384 well plate (Huberlab, Aesch, Switzerland) for drug assays. Compounds were added at indicated final concentrations in 1 % DMSO with at least six replicates for each condition. The assay plate was sealed with a clear-view sealing foil (Huberlab), and motility was captured at 37 ˚C using a live cell imaging system (Nikon TE 2000E, Hamamatsu ORCA ER camera) and then processed with the software NIS-Elements AR V4.51 and the JOBS module (Nikon). Motility was calculated relative to the DMSO control (1 %) for each time point and the highest and lowest values were excluded. Results are shown as mean ± SEM.

Bioinformatic Analysis. Genome sequences were obtained through individual project data repositories deposited on NCBI or via WormBase Parasite v19 (Howe et al., 2017). Orthologous $TRPM_{MCLZ}$ sequences were identified via BLAST searches, aligned with ClustalW, and binding pocket alignments were curated manually. For those parasitic flatworm species containing two isoforms of $TRPM_{MCLZ}$, annotation '3a' denotes the exon upstream of the second exon '3 b'. For phylogenetic analyses, TRP orthologs were identified by BLASTp search against these databases using the previously annotated *S. mansoni* TRPs (Bais and Greenberg, 2020). Putative TRPs in other species were then confirmed by reciprocal BLASTp against the *S. mansoni* predicted proteome (Buddenborg et al., 2021) and filtered for presence of at least four transmembrane domains using DeepTMHMM (Hallgren et al., 2022). Retained sequences were aligned with MUSCLE, trimmed using TrimAl with a 20 % gap threshold (Capella-Gutierrez et al., 2009), and the resulting multiple-sequence alignment was inputted into IQ-TREE (version 2.2.0 (Minh et al., 2020);) to generate a maximum likelihood tree using standard

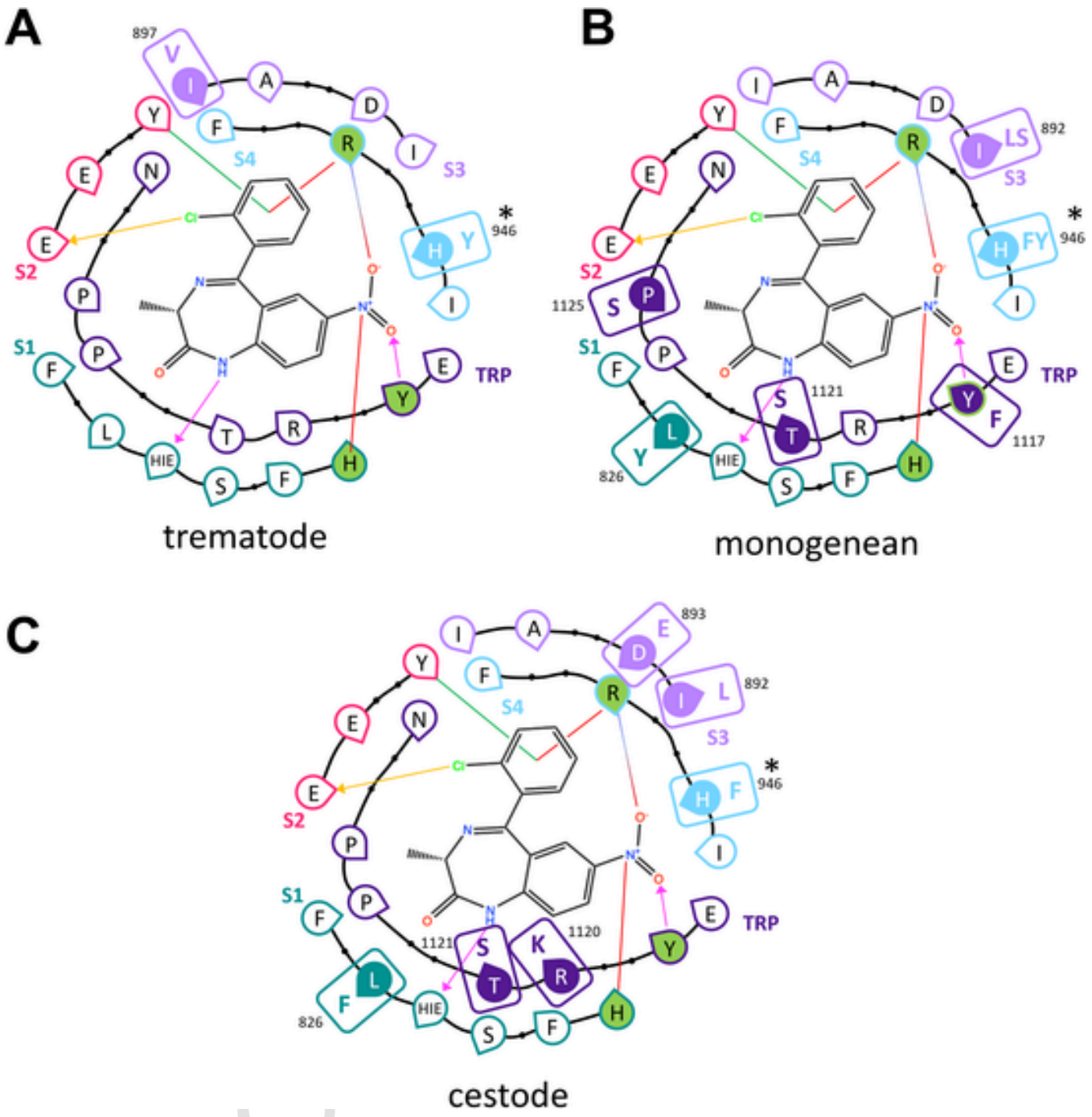

Fig. 4. Schematic of (*S*)-MCLZ binding pocket within $TRPM_{MCLZ}$ in different parasitic flatworms. Binding pocket residue identity in (**A**) generalized trematode $TRPM_{MCLZ}$, (**B**) monogenean $TRPM_{MCLZ}$, and (**C**) cyclophyllidean cestode $TRPM_{MCLZ}$. Highlighted residues (boxed) show different combinations of amino acids present at these positions. Alternative residues are shown if a variant is predicted from more than one species in same group. *, location of key residue in S4 helix that regulates schistosome $TRPM_{MCLZ}$ sensitivity to (*S*)-MCLZ. Numbering references residues found in *Sm.* $TRPM_{MCLZ}$.

model selection and 1000 bootstrap replicates. The phylogenetic tree was visualized using iTOL v7 (Letunic and Bork, 2024). A FASTA file of sequences used in generation of the tree in Fig. 1A are provided as Supplementary Dataset 1.

3. Results and discussion

TRPM channels are well represented in parasitic flatworm genomes compared with other TRP channel subfamilies. In schistosomes, there are seven predicted TRPM channels within a broader family of fifteen TRP channels comprising multiple subfamilies (TRPA, TRPC, TRPML and TRPP, Fig. 1A). The realization that two of the TRPM channels serve as targets for (*R*)-PZQ ($TRPM_{PZQ}$ (Park et al., 2019)) and (*S*)-MCLZ ($TRPM_{MCLZ}$ (Park et al., 2024)) highlights opportunity for anthelmintic design at these two targets as well as the other TRPM paralogs.

Table 1
Functional effects of various point mutants in *Sm*.TRPM$_{MCLZ}$. Indicated amino acids substitutions were profiled in a Ca^{2+} reporter assay, with the corresponding values for potency (EC_{50}) and efficacy (B_{max}) shown. *Sm*.TRPM$_{MCLZ}$ represents the wild type, reference sequence as detailed in Supplementary Dataset 2.

construct	helix	EC_{50} (μM)	B_{max} (%)
Sm.TRPM$_{MCLZ}$		1.4 ± 0.2	100
Sm.TRPM$_{MCLZ}$ [L826F]	S1	1.6 ± 0.3	85.6 ± 7.5
Sm.TRPM$_{MCLZ}$ [I892L]	S3	4.6 ± 0.5	83.1 ± 6.7
Sm.TRPM$_{MCLZ}$ [D893E]	S3	3.8 ± 0.6	82.8 ± 11.8
Sm.TRPM$_{MCLZ}$ [H946F]	S4	60.4 ± 24	43.1 ± 1.9
Sm.TRPM$_{MCLZ}$ [H946Y]	S4	21.7 ± 1.2	72.7 ± 7.0
Sm.TRPM$_{MCLZ}$ [R1120K]	TRP	7.0 ± 0.5	78.3 ± 2.6
Sm.TRPM$_{MCLZ}$ [T1121S]	TRP	3.5 ± 0.5	100.7 ± 16.0
Fh.TRPM$_{MCLZ}$ [Y994H]	S4	low activity	n/a
Eg.TRPM $_{MCLZ}$ [F952H]	S4	low activity	n/a

3.1. (*S*)-MCLZ activity against Schistosoma mansoni

(*S*)-MCLZ causes a rapid contraction of adult *S. mansoni* worms (Fig. 1B (Pax et al., 1978; Bricker et al., 1983; Thibaut et al., 2009),), with an inhibition of worm motility occurring over the low micromolar range (IC_{50} for (*S*)-MCLZ = 1.54 ± 0.09 μM (Park et al., 2024)). This potency matches the concentration-dependent activation of *S. mansoni* TRPM$_{MCLZ}$ (*Sm*.TRPM$_{MCLZ}$, gene ID *Smp_333650*) by (*S*)-MCLZ (EC_{50} = 1.42 ± 0.19 μM, Fig. 1B). (*S*)-MCLZ action on *S. mansoni* adult worms therefore correlates well with the *in vitro* sensitivity of *Sm*. TRPM$_{MCLZ}$ (Park et al., 2024). Does this correlation hold for TRPM$_{MCLZ}$ orthologs in other parasites? With the candidate target identified, there is opportunity to test whether the sensitivity of parasitic flatworm TRPM$_{MCLZ}$ orthologs corresponds with the (*S*)-MCLZ sensitivity of different parasitic flatworms.

3.2. (*S*)-MCLZ activity in other parasitic flatworms

TRPM$_{MCLZ}$ orthologs exist in other parasitic flatworms (Fig. 1A (Park et al., 2024),). We therefore profiled (*S*)-MCLZ activity in two different models: first, the liver fluke *Fasciola hepatica*, a trematode from the order *Plagiorchiida*; second, *Echinococcus multilocularis*, a cyclophyllidean cestode. The sensitivity of the TRPM$_{MCLZ}$ orthologs to (*S*)-MCLZ in these parasites was also evaluated.

In *F. hepatica* (*S*)-MCLZ was first tested against newly excysted juvenile worms (NEJs). BZQ, a recently discovered TRPM$_{PZQ}$ activator (Sprague et al., 2023b), was also used as a positive control as these trials were carried out in a TCBZ-resistant strain (due to metacercariae availability). Videos of parasite motility were recorded for each treatment, and effects on individual worms were quantified by measuring change in worm length over time. BZQ (2.5 μM, 18 h) caused worm contraction, but no contraction was observed with (*S*)-MCLZ (Fig. 2A). Next, MCLZ was tested against juvenile worms in TCBZ-sensitive strain following culture *in vitro* for 3 weeks in 50 % chicken serum. Over this time worms increase in area ~5-fold and develop structures such as a thickened tegument and branched gut (McCusker et al., 2016). Cultured juveniles were incubated for 18 h in either MCLZ (10 μM), a negative control (DMSO), or a positive control (TCBZ, 1.5 μM). As expected, TCBZ treated worms contracted but MCLZ treatment (10 μM) had little effect (Fig. 2A). Finally, (*S*)-MCLZ was tested against *F. hepatica* miracidia. While TCBZ (10 μM) caused a rapid inhibition of movement, addition of (*S*)-MCLZ (≤10 μM) or the vehicle control (DMSO) failed to impair motility Fig. 2B). Collectively, these data evidence little sensitivity toward (*S*)-MCLZ across different *F. hepatica* life cycle stages.

The *F. hepatica* TRPM$_{MCLZ}$ ortholog (*Fh*.TRPM$_{MCLZ}$, gene ID *Fh-Hic23_g5667*) was then tested for (*S*)-MCLZ sensitivity. No activation was apparent with (*S*)-MCLZ (tested at concentrations ≤100 μM, Fig. 2C). This lack of activation was consistent with the lack of (*S*)-MCLZ sensitivity observed across the different *F. hepatica* life cycle stages.

(*S*)-MCLZ activity was then examined in a cestode model in a screen of *E. multilocularis* protoscoleces. In these assays, (*R*)-PZQ was used as a positive control as it is known to cause contraction and paralysis (Fig. 3A) over a concentration range consistent with the potent activity of (*R*)-PZQ at TRPM$_{PZQ}$ (Rohr et al., 2023; Sprague et al., 2023a). No inhibition of movement was seen when (*S*)-MCLZ was added to the medium (≤100 μM). At the highest concentration (100 μM), potentiation of movement was observed (Fig. 3A).

In parallel, the TRPM$_{MCLZ}$ ortholog from *E. granulosus* (*Eg*.TRPM$_{MCLZ}$, gene ID *EgrG_001087300*) was tested for (*S*)-MCLZ sensitivity. No activity was apparent with (*S*)-MCLZ (tested at concentrations ≤100 μM, Fig. 3B). These data were consistent with the lack of (*S*)-MCLZ activity on protoscoleces *ex vivo*. Therefore, in both parasite models that have been shown here to lack sensitivity to (*S*)-MCLZ *ex vivo*, the corresponding TRPM$_{MCLZ}$ orthologs were not activated by (*S*)-MCLZ.

3.3. TRPMMCLZ binding pocket bioinformatics

Can the differences in (*S*)-MCLZ sensitivity between parasites be explained by differences in the transmembrane ligand binding pocket found in the corresponding TRPM$_{MCLZ}$ orthologs? A binding pose for (*S*)-MCLZ in *Sm*. TRPM$_{MCLZ}$ has been proposed using a compilation of docking methods and molecular dynamics (Park et al., 2024). (*S*)-MCLZ is proposed to occupy a cavity within the VSLD (S1-S4) of *Sm*. TRPM$_{MCLZ}$ that is analogous to the binding pocket of menthol in human TRPM8 and (*R*)-PZQ in TRPM$_{PZQ}$ (Park et al., 2021). (*S*)-MCLZ resides within this VSLD cavity within close proximity (5 Å) to twenty four amino acid residues (Park et al., 2024), with six residues from the S1 helix, S2 helix, S4 helix and TRP helix predicted to interact with (S)-MCLZ (Fig. 4A).

Analysis of available genomic and transcriptomic resources (see 'Methods') enabled prediction of this suite of twenty four amino acid residues across sixty-three TRPM$_{MCLZ}$ orthologs from various trematodes, monogeneans and cestodes (Supplementary Table 1). The six binding pocket residues predicted to interact with (*S*)-MCLZ (Park et al., 2024) displayed strong conservation across all these different parasites. For example, key S1, S4 and TRP residues (H831, R943, Y1117 in *Sm*. TRPM$_{MCLZ}$, colored in green in Fig. 4A) were well conserved across all TRPM$_{MCLZ}$ orthologs: H831 (S1) and R943 (S4) are completely conserved, while Y1117 (TRP) was conserved with the exception of a phenyalanine substitution in *Gyrodactylus* spp. (Supplementary Table 1). The other predicted (*S*)-MCLZ interacting residues in S1 (H827) and S2 (Y864, E868) were also well conserved.

However, changes in other residues proximal to the (*S*)-MCLZ binding pose were evident. These data are summarized in Fig. 4 to highlight binding pocket residues that differ between the various types of parasitic flatworm (Fig. 4A–C). Monogenean and cestode TRPM$_{MCLZ}$ channels displayed more variation in the (*S*)-MCLZ binding pocket, with six loci of variation unique to monogeneans (Fig. 4B) or cestodes (Fig. 4C). This number of differences would be consistent with a different binding pocket architecture and ligand binding profile compared with *Sm*. TRPM$_{MCLZ}$, potentially explaining the lack of activity of (*S*)-MCLZ in the cestode model *in vitro* and against cestode TRPM$_{MCLZ}$ (Fig. 3).

Given the known architectural mealleability of TRPM VSLD binding pockets, analyses based on bioinformatics alone remain speculative. Therefore, to provide functional insight into the effects of these differences, each of the six natural variants catalogued in cestode TRPM$_{MCLZ}$ were generated individually within the *Sm*. TRPM$_{MCLZ}$ backbone. With the exception of the S4 residue (H946 in *Sm*. TRPM$_{MCLZ}$) that is represented by a phenylalanine in cestode TRPM$_{MCLZ}$, all other mutants retained reasonable sensitivity toward (*S*)-MCLZ (Table 1). However, *Sm*. TRPM$_{MCLZ}$ [H946F] resulted in >40-fold decrease in (*S*)-MCLZ potency

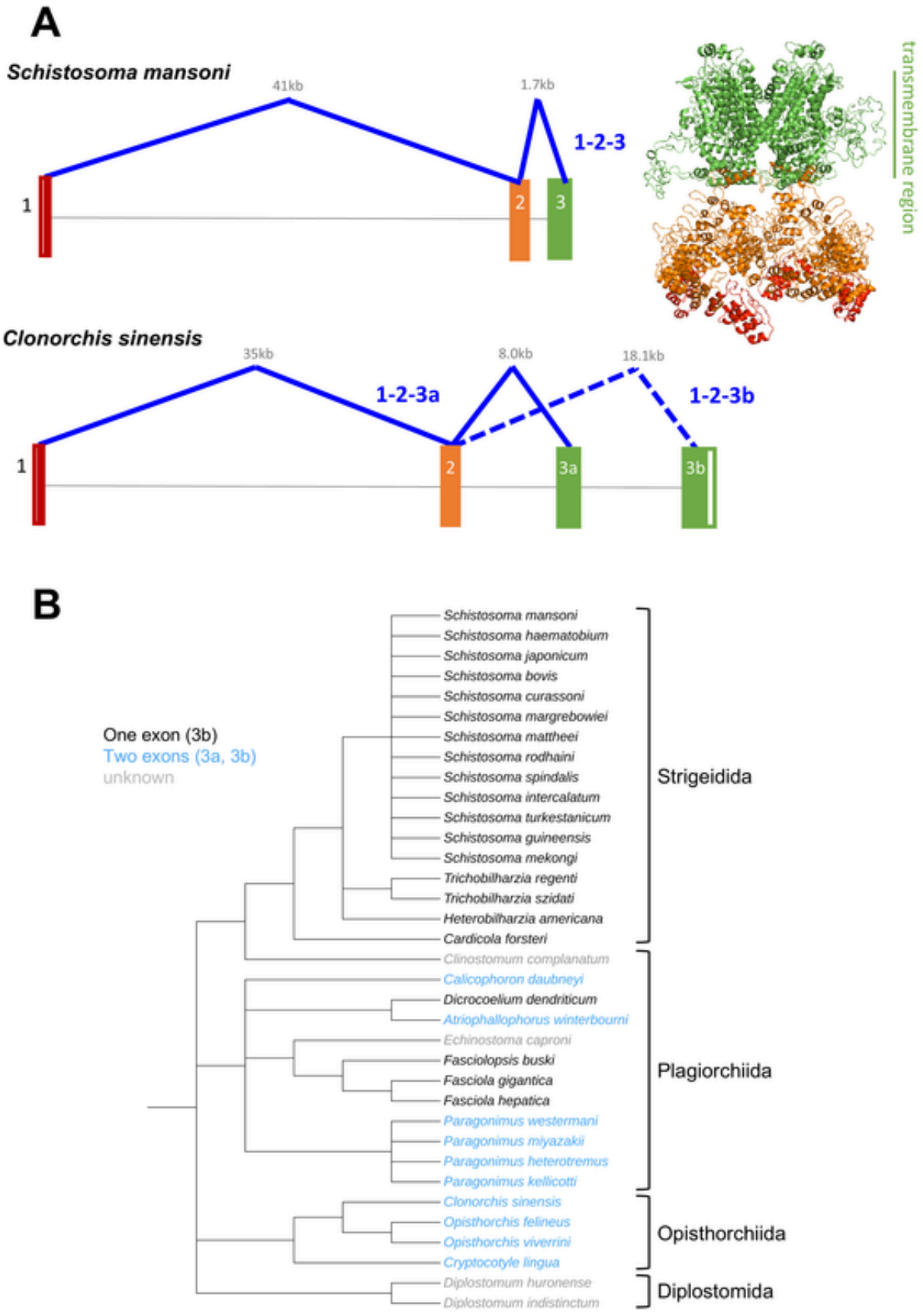
A
Schistosoma mansoni
41kb
1.7kb
1-2-3
1
2
3
transmembrane region
Clonorchis sinensis
35kb
8.0kb
18.1kb
1-2-3a
1-2-3b
1
2
3a
3b
B
One exon (3b)
Two exons (3a, 3b)
unknown
Schistosoma mansoni
Schistosoma haematobium
Schistosoma japonicum
Schistosoma bovis
Schistosoma curassoni
Schistosoma margrebowiei
Schistosoma mattheei
Schistosoma rodhaini
Schistosoma spindalis
Schistosoma intercalatum
Schistosoma turkestanicum
Schistosoma guineensis
Schistosoma mekongi
Trichobilharzia regenti
Trichobilharzia szidati
Heterobilharzia americana
Cardicola forsteri
Clinostomum complanatum
Calicophoron daubneyi
Dicrocoelium dendriticum
Atriophallophorus winterbourni
Echinostoma caproni
Fasciolopsis buski
Fasciola gigantica
Fasciola hepatica
Paragonimus westermani
Paragonimus miyazakii
Paragonimus heterotremus
Paragonimus kellicotti
Clonorchis sinensis
Opisthorchis felineus
Opisthorchis viverrini
Cryptocotyle lingua
Diplostomum huronense
Diplostomum indistinctum
Strigeidida
Plagiorchiida
Opisthorchiida
Diplostomida

Fig. 5. Identification of a possible alternate exon in a subset of trematodes. (**A**) Exon organization of *S. mansoni* $TRPM_{MCLZ}$ (top) compared with *Clonorchis sinensis* $TRPM_{MCLZ}$ (bottom). The oriental liver fluke has two predicted terminal exons (3a and 3 b), compared to a single terminal exon (3) in the blood fluke. Schematic is drawn to scale with genomic spacing of exons illustrated. (**B**) Bioinformatic analysis for the presence of the duplicated exon in different trematode groups. The duplication (blue) is present in the Opisthorchiida, *Paragonimus spp*. and two other Plagiorchiida representatives. Grey color indicates no prediction of $TRPM_{MCLZ}$ architecture based on currently available genomic sequences. Species classifications were reconstructed from the evolutionary pedigree of LifeMap (de Vienne, 2016) and visualized using the Interactive Tree of Life v7 (Letunic and Bork, 2024).

and >50 % decrease in efficacy. These data again underscore the importance of residue identity at this specific position in the S4 helix for (S)-MCLZ efficacy. It is interesting to note that the equivalent residue in $TRPM_{PZQ}$ (Y1517) engages with π-π stacking interactions with (*R*)-PZQ (Park et al., 2021), and the equivalent residue in flycatcher TRPM8 is important for binding icilin (Yin et al., 2019). Mutations at this same residue are also associated with human TRP channelopathies, further underscoring functional importance (Hofmann et al., 2017).

In trematodes, more limited variation occurred within the *Sm*. $TRPM_{MCLZ}$ pocket lining, but one of the only two variable loci was again this same S4 residue. A tyrosine residue, diagnostic of the lower sensitivity schistosome clade was present in *Trichlobilharzia* spp., *Heterobilharzia americana* as well as other schistosome species classified within the generalized 'Asian' pedigree (Lawton et al., 2011). We would therefore predict all these parasites exhibit poor sensitivity to (S)-MCLZ. A tyrosine residue was also present at this position in the Plagiorchiida, which includes both *Fasciola* spp. as well as *Paragonimus* spp. Based on mutagenesis data (Table 1 (Park et al., 2024),), one would predict that this tyrosine substitution confers lower sensitivity to (*S*)-MCLZ, consistent with the functional assay results using *F. hepatica* and *Fh*. $TRPM_{MCLZ}$ (Fig. 2). However, we note reciprocal mutation of this residue in either the *F. hepatica* backbone (*Fh*.$TRPM_{MCLZ}$ [Y994H]) or the cestode backbone (*Eg*.$TRPM_{MCLZ}$ [F952H]) did not recover significant sensitivity to (*S*)-MCLZ (Table 1). Therefore, it is likely that binding pocket size and/or architecture, in addition to the particular identity of the S4 residue, provides additional constraints for ligand engagement at $TRPM_{MCLZ}$. Other residues in the transmembrane helices do vary between all these $TRPM_{MCLZ}$ orthologs, with the current analysis only prioritizing interactions and proximity to the predicted (*S*)-MCLZ binding pose in *Sm*. $TRPM_{MCLZ}$ (Park et al., 2024).

In summary, the lack of (*S*)-MCLZ sensitivity of two $TRPM_{MCLZ}$ orthologs (*Fh*.$TRPM_{MCLZ}$, *Eg*. $TRPM_{MCLZ}$) aligns with the lack of sensitivity of these parasites to (*S*)-MCLZ. The identity of the S4 variant (F, H or Y) residue in $TRPM_{MCLZ}$, which varies in size and rotameric potential, acts as an important determinant of (*S*)-MCLZ potency and efficacy.

3.4. Exon structure of trematode TRPMMCLZ

In studying the genomic annotations of $TRPM_{MCLZ}$, we noticed a potential duplicated exon in a subset of the parasitic flatworm $TRPM_{MCLZ}$ channels. These channels included $TRPM_{MCLZ}$ orthologs from *Clonorchis sinensis, Opisthorchis* spp. and *Paragonimus* spp. $TRPM_{MCLZ}$ is typically encoded by 3 exons but these particular $TRPM_{MCLZ}$ representatives present two versions of exon 3 in their genomes (designated as exon '3a' upstream of exon '3 b', Fig. 5A). Analysis of available transcriptomes provide support for expression of either exon, rather than both, with the '1-2-3 b' configuration most closely resembling the standard (exon '1-2-3') $TRPM_{MCLZ}$ orthologs. The residues lining the binding pocket encoded in exon '3a' were unique from exon '3 b' (Supplementary Table 2). While we have not been able to confirm usage of both exons directly owing to a lack of access to biological tissue, this represents a curious observation for future study, given exon 3 encodes the entire channel domain of $TRPM_{MCLZ}$ (Fig. 5A). As such, an alternative splicing event would substantially change channel properties, comprising the VSLD binding pocket, the pore-forming domain and the carboxy terminus of this ion channel. Functionally, this could generate ion channels with completely distinct properties in those parasites that harbor this duplication (Fig. 5B).

3.5. Screening (S)-MCLZ at other schistosome TRPM channels

The absence of responses to (*S*)-MCLZ in *F. hepatica* and *E. mutilocularis* suggests there are no other targets sensitive to low concentrations of (*S*)-MCLZ in these parasites. To directly assess whether any other members of the TRPM family are activated by (*S*)-MCLZ, all seven schistosome TRPM family members (Fig. 1A) were profiled using the Ca^{2+} reporter assay. Whereas $TRPM_{PZQ}$ (*Smp_246790*) and $TRPM_{MCLZ}$ (*Smp_333650*) were both reciprocally activated by (*R*)-PZQ and (*S*)-MCLZ respectively (Park et al., 2019, 2024), none of the other predicted TRPM paralogs displayed any activity in response to either ligand (Fig. 6A). These data have an obvious caveat that no known activators of these channels have been established, so the negative data could alternatively be explained by either a lack of functional channel expression, or a lack of Ca^{2+} permeability of the other paralogs.

However, inspection of the TRPM binding pockets of the other predicted schistosome TRPM channels provides support for the suggestion that $TRPM_{MCLZ}$ is likely the sole TRPM channel activated by (*S*)-MCLZ. This is because several of the key residues implicated in (*S*)-MCLZ engagement (Fig. 4A) differ between the other TRPM paralogs. This includes the histidine residue at the key S4 position, which only occurs in *Sm*. $TRPM_{MCLZ}$ (Fig. 6B). Different residues are present at this position in the other TRPM paralogs (tyrosine in $TRPM_{PZQ}$ and *Smp_130890*, glutamic acid in *Smp_000050* and *Smp_147140*, serine in *Smp_165170* and glycine in *Smp_347080*, Fig. 6B). In addition to the S4 residue, conservation of other residues implicated to interact with (*S*)-MCLZ is poor. For example, both S1 histidine residues proposed to interact with (*S*)-MCLZ are not found in any other schistosome TRPM channel (Fig. 6B).

4. Conclusions

These data suggest the 'narrow spectrum' anthelmintic activity of MCLZ against a subset of schistosome species results from natural residue variation and the divergent architecture of the ligand binding pocket in $TRPM_{MCLZ}$ between different groups of parasitic flatworms. Understanding binding pocket variation between $TRPM_{MCLZ}$ orthologs provides a critical first step for optimizing ligand development at this new target. As recently shown with $TRPM_{PZQ}$ (Rohr et al., 2023; Sprague et al., 2023b), this insight can spur design of new anthelmintics with broader activity, as well as new chemotypes tailored for treating specific parasitic infections.

Uncited references

Bais and Greenberg, 2016; Diver et al., 2019.

CRediT authorship contribution statement

Claudia M. Rohr: Writing – review & editing, Writing – original draft, Investigation, Formal analysis, Conceptualization. **Paul McCusker:** Writing – review & editing, Writing – original draft, Investigation, Formal analysis, Conceptualization. **Marc Kaethner:** Writing – review & editing, Writing – original draft, Investigation, Formal analysis, Conceptualization. **Rebecca Armstrong:** Writing – review & editing, Writing – original draft, Investigation, Formal analysis, Conceptualization. **Emily Robb:** Writing – review & editing, Writing – original draft, Investigation, Formal analysis, Conceptualization. **Sang-Kyu Park:** Writing – review & editing, Writing – original draft, Investigation, For-

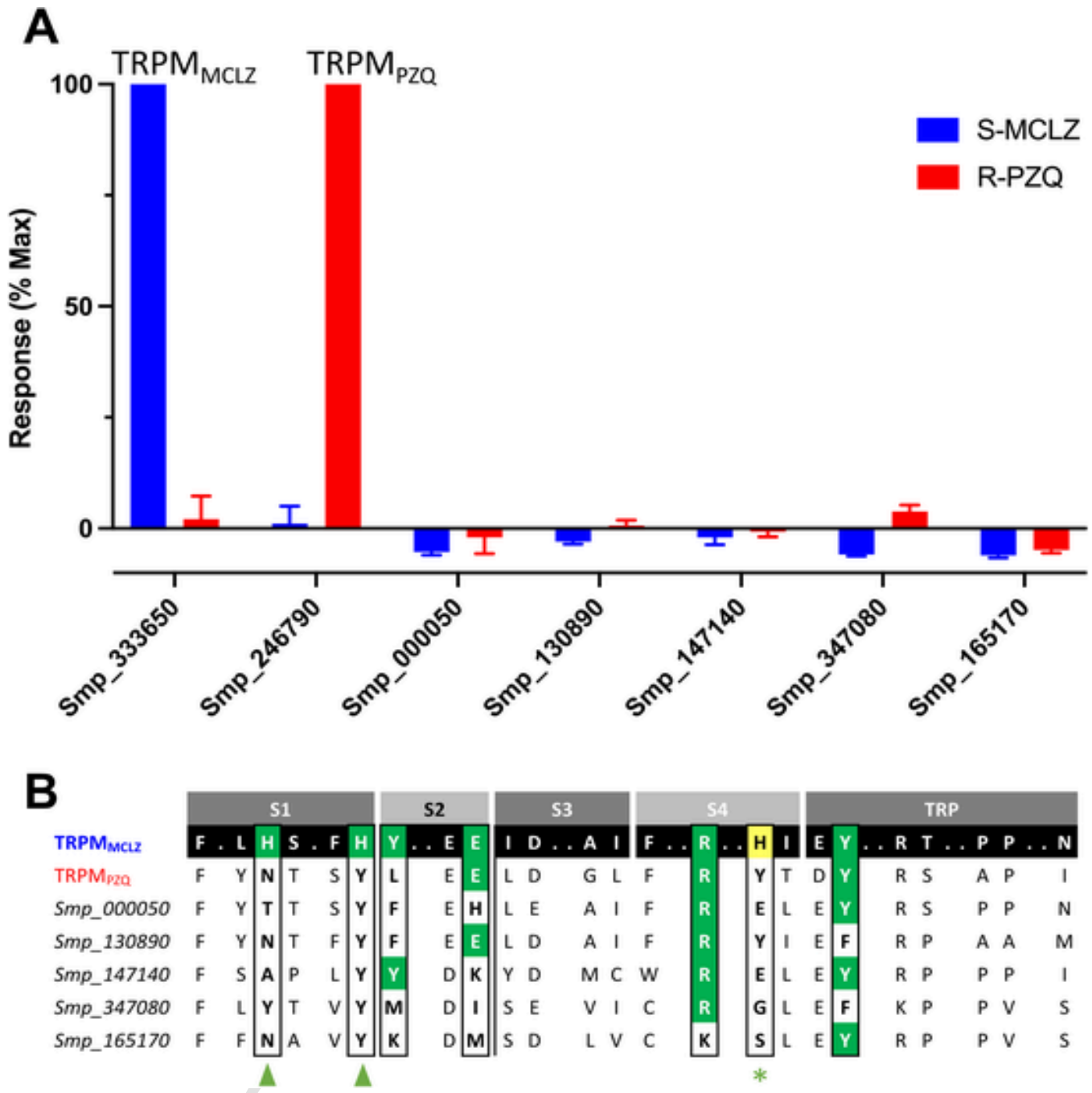

Fig. 6. Profiling (*S*)-MCLZ versus other schistosome TRPM channels. (**A**) Activity of (±)-PZQ (red) and (*S*)-MCLZ (blue) tested (both at 100 μM) using the Ca^{2+} reporter assay at each of the *S. mansoni* TRPM paralogs, including $TRPM_{PZQ}$ (*Smp_246790*) and $TRPM_{MCLZ}$ (*Smp_333650*). Peak fluorescence amplitude was collated for each assay. Note, other than for $TRPM_{PZQ}$ and $TRPM_{MCLZ}$, no positive control compounds have yet been identified that confirm functional channel expression. (**B**) Alignment of the 24 residues predicted to lie in close proximity to the binding pose of (S)-MCLZ between different schistosome TRPM channels. The six proximal residues predicted to form interactions with (S)-MCLZ (see Fig. 4) are shown in green, with conservation with other schistosome TRPM channels also highlighted in green. The residue at the key position in the S4 helix (H946 in *Sm*. $TRPM_{MCLZ}$) which regulates schistosome $TRPM_{MCLZ}$ sensitivity to (S)-MCLZ is highlighted (yellow, *). S1 residues that lack conservation between $TRPM_{MCLZ}$ and the other schistosome TRPM channels are highlighted (triangles).

mal analysis, Conceptualization. **Daniel J. Sprague:** Writing – review & editing, Writing – original draft, Investigation, Formal analysis, Conceptualization. **Aaron G. Maule:** Writing – review & editing, Writing – original draft, Investigation, Formal analysis, Conceptualization. **Mostafa Zamanian:** Writing – review & editing, Writing – original draft, Investigation, Formal analysis, Conceptualization. **Britta Lundström-Stadelmann:** Writing – review & editing, Writing – original draft, Investigation, Formal analysis, Conceptualization. **John D. Chan:** Writing – review & editing, Writing – original draft, Investigation, Formal analysis, Conceptualization. **Jonathan S. Marchant:** Writing – review & editing, Writing – original draft, Investigation, Formal analysis, Conceptualization.

Conflict of interest

The authors declare no conflicts of interest.

Acknowledgements

Schistosome-infected mice were provided by the NIAID Schistosomiasis Resource Center at the Biomedical Research Institute (Rockville, MD) through NIH-NIAID Contract HHSN272201000005I for distribution via BEI Resources. We thank Prof. Klaus Brehm (University of Würzburg) for providing fertile *E. multilocularis* metacestode material. This work was supported by the Marcus Family and NIH (R01-AI145871 to JSM, F31-AI183573 to CMR). DJS acknowledges support from NIH (T32 HL134643), the American Heart Association (24-POST1185452), and the MCW Cardiovascular Center's A.O. Smith Fellowship Scholars Program. MK and BLS acknowledge funding through the Swiss National Science Foundation (SNSF) grant nb. 310030_192072. AGM acknowledges support from the Biotechnology and Biological Sciences Research Council (BB/T002727/1). All authors would like to thank Peter McAnespie at Linden ABP Foods (Dungannon) for facilitating collection of adult liver fluke.

Appendix A. Supplementary data

Supplementary data to this article can be found online at https://doi.org/10.1016/j.ijpddr.2026.100634.

References

Andrews, P., Thomas, H., Pohlke, R., Seubert, J., 1983. Praziquantel. Med. Res. Rev. 3, 147–200.
Baard, A.P., Sommers, D.K., Honiball, P.J., Fourie, E.D., du Toit, L.E., 1979. Preliminary results in human schistosomiasis with Ro 11-3128 S Afr. Med. J. 55, 617–618.
Bais, S., Greenberg, R.M., 2016. TRP channels in schistosomes. International Journal for Parasitology Drugs and Drug Resistance 6, 335–342.
Bais, S., Greenberg, R.M., 2020. Schistosome TRP channels: an appraisal international. Journal for Parasitology Drugs and Drug Resistance 13, 1–7.
Bricker, C.S., Depenbusch, J.W., Bennett, J.L., Thompson, D.P., 1983. The relationship between tegumental disruption and muscle-contraction in *Schistosoma mansoni* exposed to various compounds zeitschrift Fur parasitenkunde. Parasitol. Res. 69, 61–71.
Buddenborg, S.K., Tracey, A., Berger, D.J., Lu, Z., Doyle, S.R., Fu, B., et al., 2021. Assembled chromosomes of the blood fluke *Schistosoma mansoni* provide insight into the evolution of its ZW sex-determination system. bioRxiv 2021.2008.2013.456314.
Capella-Gutierrez, S., Silla-Martinez, J.M., Gabaldon, T., 2009. trimAl: a tool for automated alignment trimming in large-scale phylogenetic analyses. Bioinformatics 25, 1972–1973.
de Vienne, D.M., 2016. Lifemap: exploring the entire tree of life. PLoS Biol. 14, e2001624.
Diver, M.M., Cheng, Y., Julius, D., 2019. Structural insights into TRPM8 inhibition and desensitization. Science 365, 1434–1440.
Hallgren, J., Tsirigos, K.D., Pedersen, M.D., Almagro Armenteros, J.J., Marcatili, P., Nielsen, H., et al., 2022. DeepTMHMM predicts alpha and beta transmembrane proteins using deep neural networks. bioRxiv 2022.2004.2008.487609.
Hofmann, L., Wang, H., Zheng, W., Philipp, S.E., Hidalgo, P., Cavalie, A., et al., 2017. The S4---S5 linker - gearbox of TRP channel gating. Cell Calcium 67, 156–165.
Howe, K.L., Bolt, B.J., Shafie, M., Kersey, P., Berriman, M., 2017. WormBase ParaSite - a comprehensive resource for helminth genomics. Mol. Biochem. Parasitol. 215, 2–10.
Kaethner, M., Preza, M., Kaempfer, T., Zumstein, P., Tamponi, C., Varcasia, A., et al., 2023. Establishment and application of unbiased in vitro drug screening assays for the identification of compounds against Echinococcus granulosus sensu stricto. PLoS Neglected Trop. Dis. 17, e0011343.
Lawton, S.P., Hirai, H., Ironside, J.E., Johnston, D.A., Rollinson, D., 2011. Genomes and geography: genomic insights into the evolution and phylogeography of the genus schistosoma. Parasites Vectors 4, 131.
Letunic, I., Bork, P., 2024. Interactive tree of life (iTOL) v6: recent updates to the phylogenetic tree display and annotation tool. Nucleic Acids Res. 52, W78–W82.
Marchant, J.S., 2024. Progress interrogating $TRPM_{PZQ}$ as the target of praziquantel. PLoS Neglected Trop. Dis. 18, e0011929.
McCusker, P., Armstrong, R., Wells, D., Robb, E., McVeigh, P., Maule, A., et al., 2023. In Vitro Excystment of Juvenile Fasciola Hepatica Protocolsio.
McCusker, P., Hussain, W., McVeigh, P., McCammick, E., Clarke, N.G., Robb, E., et al., 2020. RNA interference dynamics in juvenile fasciola hepatica are altered during in vitro growth and development. Int. J. Parasitol.: Drugs Drug Resist. 14, 46–55.
McCusker, P., McVeigh, P., Rathinasamy, V., Toet, H., McCammick, E., O'Connor, A., et al., 2016. Stimulating Neoblast-Like cell proliferation in juvenile fasciola hepatica supports growth and progression towards the adult phenotype in vitro. PLoS Neglected Trop. Dis. 10, e0004994.
McVeigh, P., McCammick, E.M., McCusker, P., Morphew, R.M., Mousley, A., Abidi, A., et al., 2014. RNAi dynamics in juvenile fasciola spp. liver flukes reveals the persistence of gene silencing in vitro. PLoS NTD 8, e3185.
Minh, B.Q., Schmidt, H.A., Chernomor, O., Schrempf, D., Woodhams, M.D., von Haeseler, A., et al., 2020. IQ-TREE 2: new models and efficient methods for phylogenetic inference in the genomic era. Mol. Biol. Evol. 37, 1530–1534.
Park, S.K., Friedrich, L., Yahya, N.A., Rohr, C.M., Chulkov, E.G., Maillard, D., et al., 2021. Mechanism of praziquantel action at a parasitic flatworm ion channel. Sci. Transl. Med. 13. . eabj5832.
Park, S.K., Gunaratne, G.S., Chulkov, E.G., Moehring, F., McCusker, P., Dosa, P.I., et al., 2019. The anthelmintic drug praziquantel activates a schistosome transient receptor potential channel. J. Biol. Chem. 294, 18873–18880.
Park, S.K., Sprague, D.J., Rohr, C.M., Chulkov, E.G., Petrow, I., Kumar, S., et al., 2024. The anthelmintic meclonazepam activates a schistosome transient receptor potential channel. J. Biol. Chem. 300, 105528.
Pax, R., Bennett, J.L., Fetterer, R., 1978. A benzodiazepine derivative and praziquantel: effects on musculature of *Schistosoma mansoni* and *Schistosoma japonicum*. Naunyn-Schmiedebergs Arch Pharmacol 304, 309–315.
Pica-Mattoccia, L., Ruppel, A., Xia, C.M., Cioli, D., 2008. Praziquantel and the benzodiazepine Ro 11-3218 do not compete for the same binding sites in schistosomes. Parasitology 135, 47–54.
Ramirez, B., Bickle, Q., Yousif, F., Fakorede, F., Mouries, M.A., Nwaka, S., 2007. Schistosomes: challenges in compound screening. Expet Opin. Drug Discov. 2, S53–S61.
Rohr, C.M., Sprague, D.J., Park, S.K., Malcolm, N.J., Marchant, J.S., 2023. Natural variation in the binding pocket of a parasitic flatworm TRPM channel resolves the basis for praziquantel sensitivity. Proc. Natl. Acad. Sci. U. S. A. 120, e2217732120.
Schneider, C.A., Rasband, W.S., Eliceiri, K.W., 2012. NIH image to ImageJ: 25 years of image analysis. Nat. Methods 9, 671–675.
Sprague, D.J., Kaethner, M., Park, S.K., Rohr, C.M., Harris, J.L., Maillard, D., et al., 2023a. The anthelmintic activity of praziquantel analogs correlates with structure-activity relationships at TRPM(PZQ). Orthologs ACS medicinal chemistry letters 14, 1537–1543.
Sprague, D.J., Park, S.-K., Gramberg, S., Bauer, L., Rohr, C.M., Chulkov, E.G., et al., 2023b. Target-based discovery of a broad spectrum flukicide. Nat Struct Mol Biol 2023.2009.2022.559026.
Sprague, D.J., Rohr, C.M., Marchant, J.S., 2024. TRP drop, TRP drop: a steady patter of anti-schistosomal target illumination. Front. Parasitol. 3, 1349623.
Stohler, H.R., 1979. In: Siegenthaler, W., Luthy, R. (Eds.), Ro 11-3128, a Novel Schistosomicidal Compound in Current Chemotherapy. American Society for Microbiology, pp. 147–148.
Thibaut, J.P., Monteiro, L.M., Leite, L.C., Menezes, C.M., Lima, L.M., Noel, F., 2009. The effects of 3-methylclonazepam on Schistosoma mansoni musculature are not mediated by benzodiazepine receptors. Eur. J. Pharmacol. 606, 9–16.
Wang, J., Chen, R., Collins, 3rd, J.J., 2019. Systematically improved in vitro culture conditions reveal new insights into the reproductive biology of the human parasite Schistosoma mansoni. PLoS Biol. 17, e3000254.
Yin, Y., Le, S.C., Hsu, A.L., Borgnia, M.J., Yang, H., Lee, S.Y., 2019. Structural basis of cooling agent and lipid sensing by the cold-activated TRPM8 channel. Science 363, eaav9334.